frontiers | Frontiers in Physics

TYPE Original Research
PUBLISHED 07 October 2022
DOI 10.3389/fphy.2022.1016932

EDITED BY
Wolfgang Bogner,
Medical University of Vienna, Austria

REVIEWED BY
Trevor Andrews,
Washington University in St. Louis,
United States
Tao Jin,
University of Pittsburgh, United States

*CORRESPONDENCE
Dong Liang,
dong.liang@siat.ac.cn
Yanjie Zhu,
yj.zhu@siat.ac.cn

‡These authors have contributed equally to this work

SPECIALTY SECTION
This article was submitted to Medical Physics and Imaging,
a section of the journal
Frontiers in Physics

RECEIVED 11 August 2022
ACCEPTED 23 September 2022
PUBLISHED 07 October 2022

CITATION
Liu Y, Wang W, Zheng Y, Wang H, Zheng H, Liang D and Zhu Y (2022), Magnetic resonance $T_{1\rho}$ quantification of human brain at 5.0 T: A pilot study.
Front. Phys. 10:1016932.
doi: 10.3389/fphy.2022.1016932

Magnetic resonance $T_{1\rho}$ quantification of human brain at 5.0 T: A pilot study

Yuanyuan Liu[1,2‡], Wenxin Wang[1,3‡], Yijia Zheng[1,4], Haifeng Wang[1], Hairong Zheng[1], Dong Liang[1*] and Yanjie Zhu[1*]

[1]Paul C. Lauterbur Research Center for Biomedical Imaging, Shenzhen Institute of Advanced Technology, Chinese Academy of Sciences, Shenzhen, China, [2]National Innovation Center for Advanced Medical Devices, Shenzhen, China, [3]Shenzhen College of Advanced Technology, University of Chinese Academy of Sciences, Shenzhen, China, [4]Chongqing University of Technology, Chongqing, China

MR quantitative T1ρ mapping has gained increasing attention due to its capability to study low-frequency motional processes and chemical exchange in biological tissues. At ultra-high fields, the chemical exchange and proton diffusion in biological tissues should be more prominent. In this study, for the first time, we aim to test the feasibility of brain $T_{1\rho}$ mapping at 5.0 T MR scanner and compare the $T_{1\rho}$ values estimated using 3.0 T and 5.0 T scanners. Preliminary experimental results show that 5.0 T achieves $T_{1\rho}$-weighted images with a higher signal-to-noise ratio than those acquired at 3.0T. The SNR benefit at 5.0 T is more obvious in high-resolution imaging. The $T_{1\rho}$ quantifications at 5.0 T are: Corpus callosum (67.4 ± 1.9 ms), Corona radiate (71.5 ± 1.8 ms), Superior frontal gyrus (67.6 ± 2.5 ms), Putamen (58.9 ± 1.2 ms), Centrum semiovale (84.0 ± 6.3 ms). Statistical analysis results indicate that the $T_{1\rho}$ values at 5.0 T show no significant difference with those obtained at 3.0 T (all $p > 0.05$). The interfield agreements in terms of $T_{1\rho}$ values between 3.0 T and 5.0 T were substantial (all ICCs >0.7). The coefficients of variation for $T_{1\rho}$ measurements from 3.0 T to 5.0 T were all less than 6.50% (2.28%–6.32%).

KEYWORDS
5.0 T, brain, ultra-high field strength, quantitative imaging, $T_{1\rho}$

Introduction

Magnetic spin-lattice relaxation in the rotation frame (referred to as $T_{1\rho}$) is an emerging technique to assess neurodegenerative diseases [1]. Relative to the conventional T_1 and T_2 relaxations, $T_{1\rho}$ provides a more specific probe of motional interactions related to the exchanges that are on the time scale of the reciprocal of the spin lock field strength. It is sensitive to the local tissue microenvironment and microstructure, such as the pH and glucose levels. Previous studies have demonstrated that proton exchange between bulk water and labile protons of protein or metabolites is an important contributor to the low-frequency $T_{1\rho}$ dispersion in biological tissue [2–5]. Therefore, $T_{1\rho}$ has been considered a potential biomarker for the evaluation and early diagnoses of degenerative neurologic diseases, such as multiple sclerosis [6–8], Alzheimer's disease [9–11], Parkinson disease [12–14], and stroke [15,16].

$T_{1\rho}$ quantification is performed by fitting a series of $T_{1\rho}$-weighted images acquired at varying spin-lock durations (TSL), which can be obtained using most magnetic resonance imaging (MRI) sequences by including a spin-lock preparation pulse at the beginning of the sequence. The $T_{1\rho}$ imaging technique is sensitive to the B_0 and B_1 field inhomogeneities and usually has a high specific absorption rate (SAR) due to the spin-lock pulse. Therefore, most $T_{1\rho}$ studies were performed at typically 1.5 T or 3.0 T fields, and human studies of $T_{1\rho}$ quantification at ultra-high fields were rarely reported [17–19]. At the ultra-high field, chemical exchanges between sites of different chemical shifts increase rapidly with field strength and may significantly contribute to the rotating frame relaxations [20]. $T_{1\rho}$ relaxation occurs in response to the chemical exchange between the groups of spins, which depends on chemical shift, temperature, exchange rate of the exchanging spins, etc. [21]. It is hence well suited for probing the metabolic information at higher magnetic field strengths [18,22]. Furthermore, high-resolution $T_{1\rho}$ quantification can be achieved using an ultra-high field MR scanner with a high signal-to-noise ratio (SNR) and affords improved morphological detail compared to imaging at lower-field strength [7] in an effort to improve visualization of brain lesions.

Last year, the first 5.0 T ultra-high field whole-body MR system (Jupiter, United Imaging Healthcare, Shanghai, China) was delivered. Compared with the 7.0 T ultra-high field system, the magnetic field strength of 5.0 T system has fewer SAR and field inhomogeneity. These advantages may bring benefits to brain $T_{1\rho}$ quantification. We implemented a three-dimensional (3D) $T_{1\rho}$ mapping sequence in this system, using a spin-lock $T_{1\rho}$ preparation pulse followed by a gradient recalled echo (GRE) readout, and applied it to imaging the brain of healthy volunteers. In this study, we will report the $T_{1\rho}$ quantification of the human brain at 5.0 T for the first time. Also, the SNR and spatial resolution gains of brain $T_{1\rho}$ images obtained from 5.0 T are demonstrated, and corresponding $T_{1\rho}$ values obtained from 5.0 T are compared with those obtained from 3.0 T.

Materials and methods

Subjects

The experiments were approved by the local Institutional Review Board (IRB). Twelve healthy volunteers (10 males, age: 30 ± 5 years; 2 females, age: 28 ± 4 years) were recruited in this study, and informed consent was obtained from each volunteer before the scan. All subjects participated in this study were scanned at a 5.0 T scanner (Jupiter, United Imaging Healthcare, Shanghai, China) and a 3.0 T scanner (uMR 890, United Imaging Healthcare, Shanghai, China). A modified $T_{1\rho}$ preparation pulse sequence based on a previously reported sequence was used [17].

Imaging sequence

The imaging sequence is depicted in Figure 1. The pulse sequence starts with a 90-degree RF pulse followed by crusher gradients to reset the net magnetization, which assures the signal is constant at the beginning of $T_{1\rho}$ preparation pulse [23]. The following recovery time (T_{rec}) allows the recovery of the magnetization before the $T_{1\rho}$ preparation pulse and the acquisition. An adiabatically prepared constant-amplitude on-resonant spin-lock preparation pulse is used for $T_{1\rho}$ preparation [17], which is robust to B_0 and B_1 inhomogeneities. It consists of a rectangular locking pulse sandwiched by an adiabatic half passage (AHP) pulse and a reverse adiabatic half passage (RAHP) pulse[24,25]. The adjusted hyperbolic secant pulses are used as the AHP and RAHP. After the $T_{1\rho}$ preparation pulse, the residual transverse magnetization is destroyed by a gradient crusher. Then a 3D segmented radiofrequency gradient echo (GRE) sequence is employed for signal acquisition using the centric phase encoding order [26,27].

The 3D $T_{1\rho}$ imaging was performed with spin-lock pulse amplitude B_{1sl} = 500 Hz and TSL = 0, 25, 45, and 65 ms at the 5.0 T and 3.0 T scanners. The 5.0 T MR scanner used a local quadrature birdcage transmit and 48-channel receiver head coil [28]. At the 3.0 T MR scanner, a commercial 32-channel receiver head coil (Rx: 32 channel) was used for $T_{1\rho}$ imaging. Three datasets were acquired for each subject at each scanner. Two datasets were acquired with a regular resolution of $1 \times 1 \times 3$ mm^3 in the sagittal and coronal orientations, respectively. Another was acquired with a high resolution of $0.65 \times 0.65 \times 2.5$ mm^3 in the transverse orientation. The imaging parameters are depicted in Table 1.

Data analysis

All $T_{1\rho}$ quantification and analysis were performed in Matlab R2017b (MathWorks, Natick, MA, United States). The $T_{1\rho}$ maps were estimated using the exponential model [29,30] by fitting the $T_{1\rho}$-weighted images with different TSLs pixel-by-pixel:

$$M_n = M_0 exp\left(-TSL_n / T_{1\rho}\right)_{n=1,2,\ldots,N} \tag{1}$$

where M_n is the image intensity obtained at varying TSLs, M_0 is the baseline image intensity without applying the spin-lock pulse. $T_{1\rho}$ map was estimated using the nonlinear least-squares fitting method with the Levenberg–Marquardt algorithm [31] from the $T_{1\rho}$-weighted images.

Five regions of interest (ROIs) were manually drawn on the images of each volunteer by two independent readers

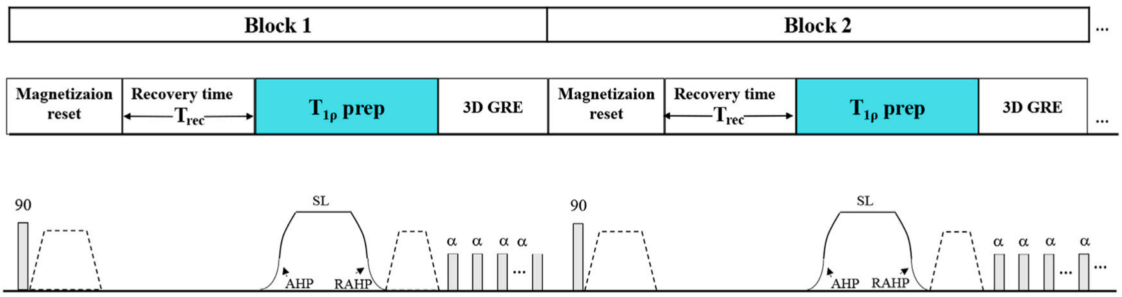

FIGURE 1
The timing diagram of the 3D $T_{1\rho}$ imaging sequence. The $T_{1\rho}$ preparation pulse was accomplished using an adiabatically prepared constant-amplitude on-resonant spin-lock approach to compensate for the B_0 and B_1 inhomogeneities at 5.0 T.

TABLE 1 Imaging parameters for $T_{1\rho}$ quantification of the human brain at 5.0 T and 3.0 T

	Regular resolution		High resolution	
	3.0 T	**5.0 T**	**3.0 T**	**5.0 T**
Coil	32-ch head	48-ch head	32-ch head	48-ch head
FOV (mm^2)	240 × 200×30	240 × 200×30	200 × 200×24	200 × 200×24
Voxel size (mm^3)	1 × 1×3	1 × 1×3	0.65 × 0.65×2.5	0.65 × 0.65×2.5
TR/TE (ms)	5.55/2.00	7.48/3.70	7.89/3.90	7.86/3.90
ETL length	50	50	50	50
Bandwidth (Hz/pixel)	500	500	500	500
Spin-lock frequency (Hz)	500	500	500	500
TSLs (ms)	0,25,45,65	0,25,45,65	0,25,45,65	0,25,45,65
Phase encoding oversampling factor	0.15	0.15	0	0
Slice oversampling factor	0.1	0.1	0	0
Block time (ms)[a]	1200	1800	1200	2000
Scan time (mins)	13:20	19:82	13:32	22:32

[a]Due to system hardware constraints, the block time for imaging at 5.0 T was set longer in the high-resolution scenario than that in the regular resolution scenario.

(with 5-year experience in neural imaging), including Corpus callosum, Corona radiate, Superior frontal gyrus, Putamen, and Centrum semiovale. The average $T_{1\rho}$ value in each ROI was calculated, and the correlation of the $T_{1\rho}$ measurements between 3.0 T and 5.0 T was analyzed.

The SNRs of $T_{1\rho}$-weighted images obtained from 5.0 T were also calculated and compared with those obtained from 3.0 T. The SNR was defined as the ratio between the mean value of the imaging regions and the standard deviation (SD) of the background noise [32]. To reduce the subject bias, four ROIs were drawn on each slice to calculate the noise SD and the SNR. Final SNR (denoted as $SNR_{T1\rho\text{-}w}$) was calculated as the average of these four SNRs. Mean values and SDs of $SNR_{T1\rho\text{-}w}$ were computed for all the volunteers in each orientation.

Statistical analysis

The difference and consistency of $T_{1\rho}$ values measured at 3.0 T and 5.0 T were statistically compared using the Mann-Whitney *U* test. The intraclass correlation coefficients (ICCs) and Bland–Altman analysis were used to evaluate the interfield agreements and to determine whether there were significant differences in terms of $T_{1\rho}$ values between 3.0 T and 5.0 T. The interfield agreement was considered to be poor for ICCs = 0.0–0.2, fair for ICCs = 0.2–0.4, moderate for ICCs = 0.4–0.6, substantial for ICCs = 0.6–0.8, and excellent for ICCs = 0.8–1.0. $p < 0.05$ was considered statistically significant. The coefficient of variation ($CV = std_{T1\rho}/mean_{T1\rho}$) was used to assess the variability and reliability of $T_{1\rho}$ values measured at 3.0 T and 5.0 T. CVs <15%, between 15% and 35% and >35% were considered

10.3389/fphy.2022.1016932

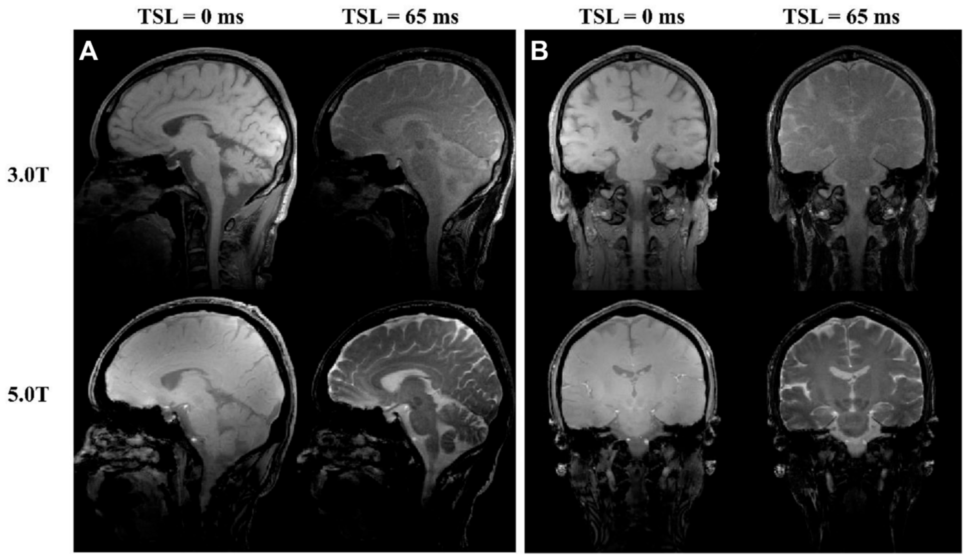

FIGURE 2
The $T_{1\rho}$-weighted images with different TSLs collected at 3.0 T and 5.0 T.

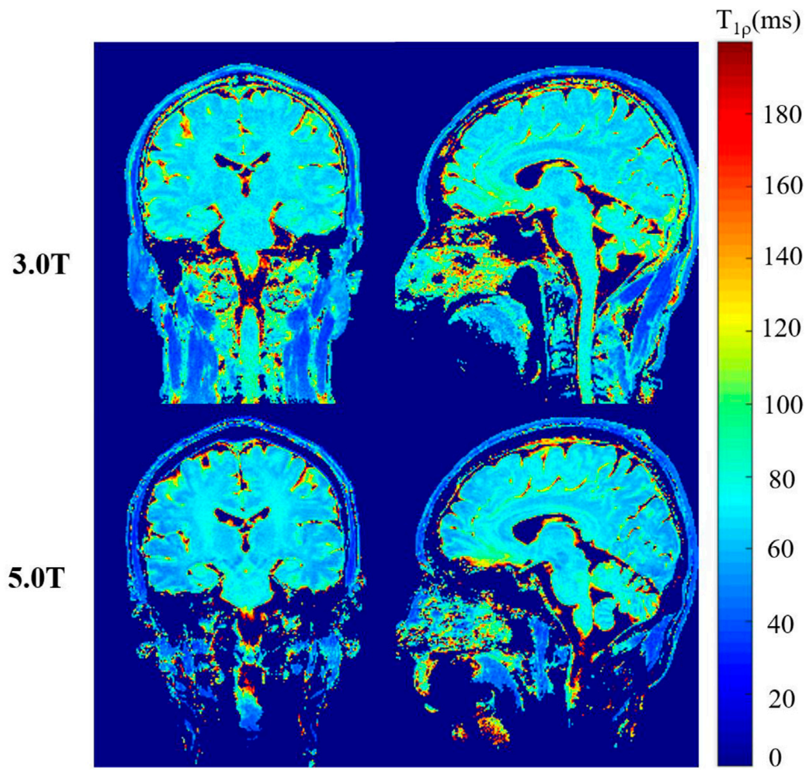

FIGURE 3
The $T_{1\rho}$ maps obtained at 3.0 T and 5.0 T.

10.3389/fphy.2022.1016932

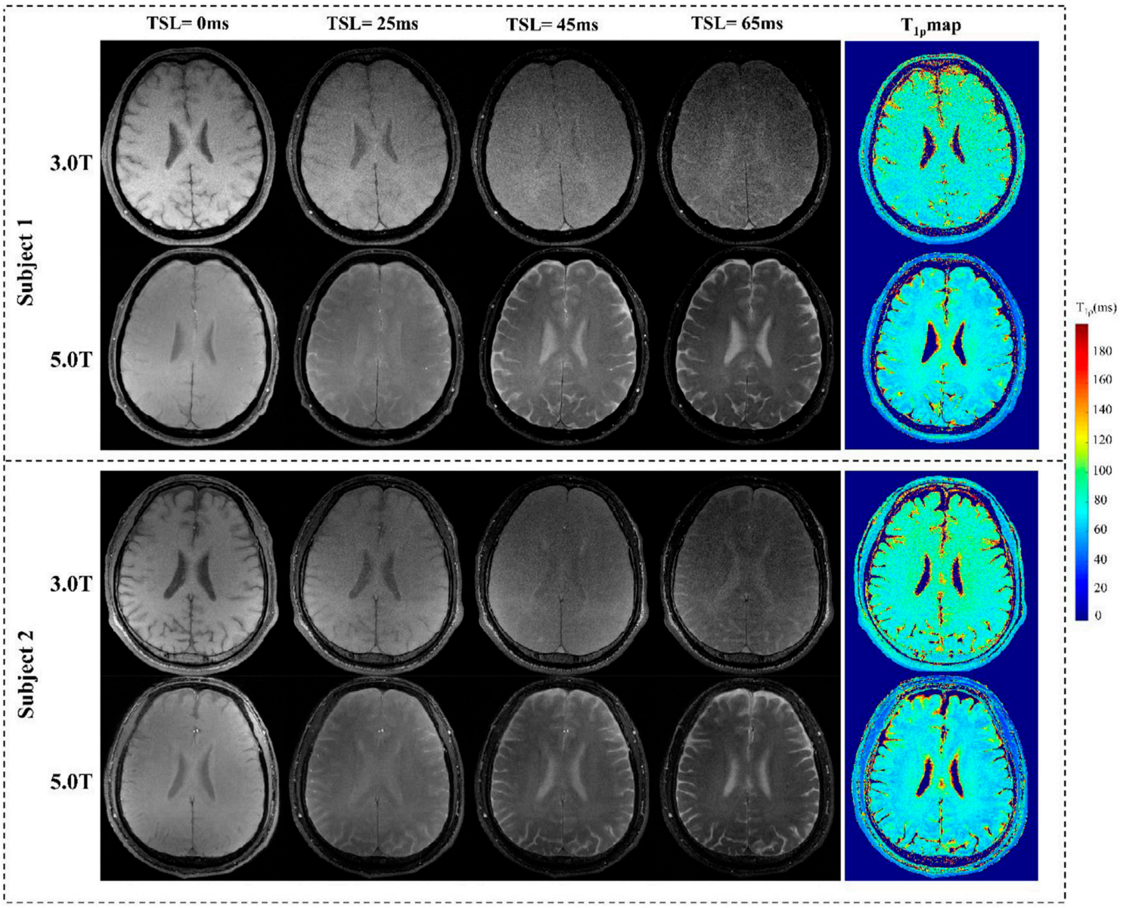

FIGURE 4
$T_{1\rho}$-maps estimated from datasets collected at 3.0 T and 5.0 T.

to be small, moderate, and large variability. Statistical analyses were performed using SPSS 25.0 (IBM, Armonk, NY) and MedCalc 20.0.22 (MedCalc Software, Mariakerke, Belgium).

Results

Imaging with regular resolution

Figure 2 shows the representative $T_{1\rho}$-weighted images at TSL = 0 and 65 ms of one subject with the regular resolution at 3.0 T and 5.0 T in the sagittal and coronal orientations, respectively. The noticeable difference between the image contrasts of 3.0 T and 5.0 T might be due to the change of relaxation time with the field strength. In addition, visible noise can be observed in the $T_{1\rho}$-weighted images at 3.0 T, especially at TSL = 65 ms, since the signal attenuates with the increase of TSL. The corresponding $T_{1\rho}$ maps of the above $T_{1\rho}$-weighted images are shown in Figure 3. These maps show extensive spatial similarities present between 3.0 T and 5.0 T $T_{1\rho}$ values for the same volunteers, except that the $T_{1\rho}$ maps at 3.0 T are a little noisier than those at 5.0 T.

Imaging with high resolution

Figure 4 shows $T_{1\rho}$-weighted images of different TSLs and the corresponding $T_{1\rho}$ maps in the high-resolution scenario for an axial slice from two subjects acquired at 3.0 T and 5.0 T. Similar conclusions to the regular scenario can be obtained. Furthermore, the SNRs of $T_{1\rho}$-weighted images obtained at 3.0 T drop significantly due to the increased resolution. As the signal decays exponentially along the TSL direction, some image details are almost drowned out by noise, especially at longer TSLs. Correspondingly, the $T_{1\rho}$ maps also seem noisy. However, the $T_{1\rho}$-weighted images obtained at 5.0 T still show good image detail with reasonable SNRs, and the image quality of $T_{1\rho}$ maps is also improved.

TABLE 2 Average $T_{1\rho}$ values of selected ROIs and the corresponding *p*-values at 3.0 T and 5.0 T

		3.0 T	5.0 T	ICC	LCI	UCI	*p*-value
Regular resolution	Corpus callosum	66.8 ± 2.3	67.2 ± 1.9	0.730	0.499	0.865	0.258
	Corona radiate	71.7 ± 1.9	71.5 ± 1.7	0.725	0.466	0.869	0.243
	Superior frontal gyrus	67.6 ± 2.1	68.1 ± 2.4	0.788	0.576	0.901	0.342
	Putamen	59.2 ± 1.5	58.7 ± 1.3	0.741	0.461	0.882	0.399
High resolution	Centrum semiovale	84.0 ± 4.7	83.5 ± 5.3	0.768	0.542	0.890	0.541

TABLE 3 The average SNR of the $T_{1\rho}$-weighted images obtained at 3.0 T and 5.0 T

	Orientation[a]	3.0 T	5.0 T	*p*-value
Regular resolution	cor	83.7 ± 9.6	99.7 ± 17.1	0.016
	sag	80.1 ± 10.4	90.4 ± 12.6	0.043
High resolution	tra	25.9 ± 3.0	38.0 ± 5.5	<0.001

[a]Cor, coronal plane, sag, sagittal plane, tra, transverse plane.

$T_{1\rho}$ measurements and signal-to-noise ratio analysis

The $T_{1\rho}$ values in the tissue compartments of the selected ROIs at 5.0 T and 3.0 T are shown in Table 2. There was no significant difference between the $T_{1\rho}$ values obtained at 5.0 T and 3.0 T (all $p >$ 0.05). The ICCs for evaluating the interfield agreements are also shown in Table 2. LCI and UCI are the abbreviations of the lower and upper bounds of the 95% confidence interval. The ICCs of $T_{1\rho}$ values in all tissue compartments between 3.0 T and 5.0 T were as follows: $ICC_{Corpus\ callosum}$ = 0.730 [95% confidence interval (CI): 0.499–0.865]; $ICC_{Corona\ radiate}$ = 0.725 (95% CI:–0.466–0.869); $ICC_{Superior\ frontal\ gyrus}$ = 0.788 (95% CI: 0.576–0.901); $ICC_{Putamen}$ = 0.788 (95% CI: 0.461–0.882) and $ICC_{Centrum\ semiovale}$ = 0.768 (95% CI: 0.542–0.890). All ICCs between the 3.0 T and 5.0 T were >0.7, indicating substantial agreements.

The SNR of the $T_{1\rho}$-weighted images obtained at 5.0 T and 3.0 T are shown in Table 3. As expected, the image SNR at 5.0 T was higher than that at 3.0 T, and significant differences were seen between the SNRs obtained at 5.0 T and 3.0 T, with $p <$ 0.05 for all imaging scenarios. On average, with the regular resolution, the SNR of the $T_{1\rho}$-weighted images obtained at 5.0 T was 15.67% higher than that at 3.0 T, and this value increased to 46.6% in the high-resolution scenario.

The coefficient of variation between the 3.0 T and 5.0 T $T_{1\rho}$ values for five selected ROIs are shown in Table 4. For 3.0 T, the CVs of $T_{1\rho}$ values for Corpus callosum, Corona radiate, Superior frontal gyrus, Putamen, Centrum semiovale were 3.42%, 2.70%, 3.14%, 2.58%, respectively, and the CVs of $T_{1\rho}$ values from 5.0 T were 2.79%, 2.36%, 3.48%, 2.28%. Based on the above results, the variability of $T_{1\rho}$ values at different field strengths for five selected ROIs was determined as small (CV < 15.0%).

TABLE 4 The Coefficient of Variation (%) of $T_{1\rho}$ values for selected ROIs at 3.0 T and 5.0 T

		3.0 T	5.0 T
Regular resolution	Corpus callosum	3.42	2.79
	Corona radiate	2.70	2.36
	Superior frontal gyrus	3.14	3.48
	Putamen	2.58	2.28
High resolution	Centrum semiovale	5.54	6.32

The Bland-Altman plots of the mean interfield differences of $T_{1\rho}$ values ($T_{1\rho}$ difference = $T_{1\rho,3.0\ T}$- $T_{1\rho,5.0\ T}$) for the five tissue compartments in the aforementioned ROIs are shown in Figure 5, and the mean interfield differences of $T_{1\rho}$ values are as follows: $T_{1\rho}$ difference of Corpus callosum: mean ±1.96SD: −3.4–2.5 ms, bias: −0.4361 ms, 95% CI: −1.0214, 0.1493; $T_{1\rho}$ difference of Corona radiate: mean ±1.96SD: −2.6–2.7 ms, bias: 0.0616 ms, 95% CI: −0.5006, 0.6238; $T_{1\rho}$ difference of Superior frontal gyrus: mean ±1.96SD: −3.3–2.3 ms, bias: −0.4864 ms, 95% CI: −1.0732, 0.1004; $T_{1\rho}$ difference of Putamen: mean ±1.96SD: −1.4–2.4 ms, bias: 0.4784 ms, 95% CI: −0.0818, 0.8750; $T_{1\rho}$ difference of Centrum semiovale: mean ± SD: −4.7–6.0 ms, bias:0.6504 ms, 95% CI: −0.4798, 1.7806.

Discussion

In this study, we demonstrated the feasibility of brain $T_{1\rho}$ quantification at 5.0 T and compared the $T_{1\rho}$ values to 3.0 T in healthy volunteers. $T_{1\rho}$ mapping at higher field strengths benefits from increased SNR and chemical exchange, resulting in its increased sensitivity to exchange effects, such as changes in macromolecule concentrations. In previous studies, $T_{1\rho}$ mapping at 7.0 T has shown great potential in studying the loss of proteoglycan and improving differentiation between knees with cartilage lesions and controls, and it is also promising for glucose metabolism studies in detecting intracerebral regions of increased glucose concentration [18,33]. However, SAR limits

10.3389/fphy.2022.1016932

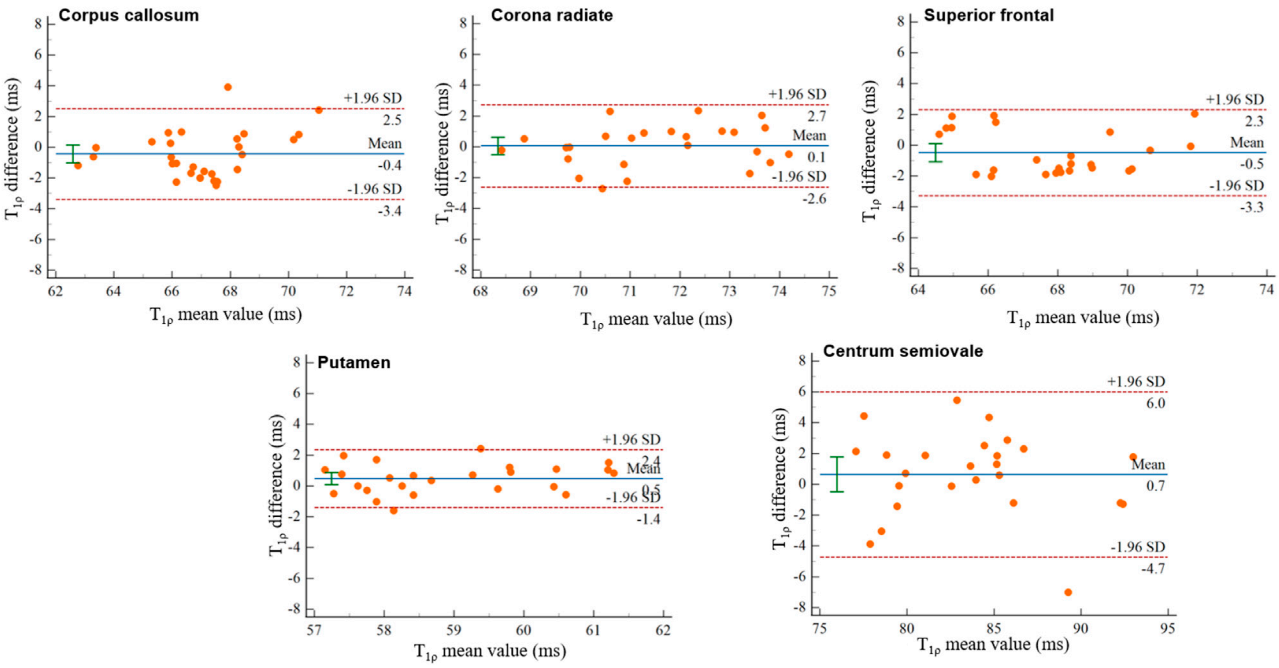

FIGURE 5
Bland–Altman plots of $T_{1\rho}$ difference values at 5.0 T relative to the $T_{1\rho}$ values at 3.0 T in the Corpus callosum, Corona radiate, Superior frontal gyrus, Putamen, and Centrum semiovale. The solid and dashed lines in the Bland-Altman plots represent the bias and ±1.96 × standard deviation, respectively.

should be carefully taken into account since the spin lock pulse requires a large amount of RF energy. Relative to 7.0 T, $T_{1\rho}$ mapping at 5.0 T has met less resistance due to lower SAR of spin lock pulse. In addition, the use of the adiabatically prepared spin-lock preparation pulse can compensate for the B_0 and B_1 inhomogeneities at 5.0 T, which are also lower than those at 7.0 T. Thus, we can obtain reliable $T_{1\rho}$ maps of the brain. To our knowledge, this is the first depiction of brain $T_{1\rho}$ mapping at 5.0 T.

High-resolution anatomical images are desirable for better clinical diagnostic details and clearer visualization of morphological abnormalities. Additionally, it hold great potential for investigation and characterization of various pathological processes. For example, demyelination and axonal loss across various brain regions are prevalent at very early stages of multiple sclerosis [7]. These high-resolution images can improve gray matter and white matter differentiation, in an effort to classify the location of lesions in relation to the cortical/subcortical boundary [34]. While in the case of lower resolution, effects of partial of skull with this free fluid would be increased and could confound interpretation of results.

Our experimental results showed that the image SNRs of $T_{1\rho}$-weighted images were significantly improved at 5.0 T, and the improvement became more obvious in the high-resolution scenario. This result was in good concordance with previous studies [34–36]. Since SNR is linearly proportional to the magnetic field strength, ultra-high field MRI affords higher spatial resolution, allowing for the visualization of small anatomic structures not previously appreciated at lower magnetic field strengths. As shown in Table 2, the $T_{1\rho}$ values of the brain obtained at 5.0 T are not significantly different from those obtained at 3.0 T. This indicates that the $T_{1\rho}$ values obtained at 5.0 T can be utilized for brain investigation, which is valuable for longitudinal investigation and comparison. Although increasing the number of averages will increase the SNR, it also enables exponential increase in the scan time. However, it may be also hard to use a different number of averages to make the scanning time of 3.0 T equal to 5.0 T. We calculated the SNR per unit of time for images at 5.0 T and 3.0 T respectively by dividing the SNR by the square root of the scanning time. Since the TE of imaging at 5.0 T is different from that at 3.0 T in the regular resolution scenario, due to different duration, gradient ramp and gradient amplitude of the readout gradient, we calculated the SNR per unit of time for images in the high resolution scenario for fair comparison. According to the SNR results in Table 3, the SNR per unit of time for images collected at 5.0 T is also higher than that at 3.0 T, with the value of 8.01 (s^{-1}) at 5.0 T, and 7.05 (s^{-1}) at 3.0 T, respectively.

TABLE 5 $T_{1\rho}$ values for white matter and gray matter at different magnetic field strengths.

Magnetic field strength (T)	Authors	$T_{1\rho}$ values (ms)	
		White matter	Gray matter
1.5	[12]	80.5 ± 1.4	87.5 ± 1.2
	[10]	82.8 ± 1.3	86.4 ± 4.4
	[6]	76.7 ± 1.6	78.2 ± 1.3
3	[7]	80.4 ± 3.3	88.9 ± 3.4
	Our study	77.52 ± 1.1	80.78 ± 1.2
4	[44]	85.6 ± 2.4	77.7 ± 1.4
4.7	[45]	85–93	—
	[4] [a]	—	63 ± 2
5	Our study	76.07 ± 1.8	80.1 ± 1.7
7	[19]	50–100	
9.4	[17]	46.47 ± 1.56	53.42 ± 1.32

[a]Due to the limited literatures on $T_{1\rho}$ mapping in the human brain, $T_{1\rho}$ values of tissues for rats were added as a reference.

In this study, since the imaging sequence contains the long-duration $T_{1\rho}$-preparation pulse, the energy deposited into tissues needs to be addressed, especially for the ultra-high field MR systems. According to previous studies [37–39], the SAR for a single pulse used in the sequence can be estimated as:

$$\mathrm{SAR}_{\tau/\alpha} = f\left(\frac{3\mathrm{ms}}{\tau}\right)^2 (\alpha/90°)^2 SAR_{3ms/90°} \quad (2)$$

where τ is the duration (in ms), α is the flip angle, f is a pulse shape factor determined by the type of pulse used, which equals 1 for a hard pulse, or equals 0.67 for a Gaussian pulse, or equals 2 for a sinc pulse. $\mathrm{SAR}_{3ms/90°}$ denotes the SAR for a 90°hard pulse with a duration of 3 ms. $SAR_{3ms/90°}$at 3.0 T for the head model was estimated between 0.242 W/kg (1.5 T) and 2.16 W/kg (4.1 T), and $SAR_{3ms/90°}$at 5.0T for the head model was slightly larger than 3.3 W/kg (4.7 T). The average SAR delivered for the pulse sequence is the sum of energy absorbed by each RF pulse divided by the total time to acquire the image:

$$\mathrm{SAR} = \frac{\sum_{n=1}^{N} \mathrm{SAR}_{\tau_n/\alpha_n} \times \tau_n}{T_{total}} \quad (3)$$

where $\mathrm{SAR}_{\tau/\alpha}$ is calculated using Eq. 2, SAR denotes the average delivered SAR over the total time period T_{total}, N denotes the number of RF pulses. The Food and Drug Administration (FDA) mandated maximum SAR level that equals 3W/kg of the head during the extremities averaged over 10 min. In this study, the average SAR delivered to the brain with TSL = 65 ms approximately 2.68 W/kg at 5.0T and between 0.22 W/kg and 1.98 W/kg at 3.0 T.

In this study, TSL times were chosen empirically based on hardware limitations. The allowed maximum RF duration depends on the RF hardware of the system. In previous studies [6,39–41], the $T_{1\rho}$-weighted images were produced by using an RF pulse cluster (e.g. $90°_{+x}$–SL_{+y} –$180°_{+y}$–SL_{-y} –$90°_{+x}$), it is easy to set the TSL to 100 ms due to using the composite SL pulses. In the UIH MR scanner, the deadtime between two pulses is 200us, which is much larger than other commercial MR scanners. The dephasing during the deadtime will affect the image quality of $T_{1\rho}$-weighted images and may result in inaccurate $T_{1\rho}$ mapping. To resolve this problem and to compensate for the B_0 and B_1 inhomogeneity, we used a single pulse to improve the robustness of $T_{1\rho}$ imaging. The maximum duration allowed of a single pulse is around 80 ms, both on the 3.0 T and 5.0T UIH MR scanners. Got rid of the time for AHP and RAHP, the maximum TSL used was 65 ms in our study. In our future work, optimized $T_{1\rho}$ preparation pulses with longer TSL and insensitive to B_0 and B_1 field inhomogeneity will be studied.

Although several studies of knee cartilage showed that 7.0 T $T_{1\rho}$ values were slightly lower than 3.0 T $T_{1\rho}$ values [33,42], the dependence between the $T_{1\rho}$ value and the B_0 field strength is not very clear for brain tissues. As is shown in Table 5, we listed the $T_{1\rho}$ values of white matter and gray matter at different field strengths reported in previous studies. The $T_{1\rho}$ values of white matter and gray matter at 3.0 T in our study are consistent with previous studies ($T_{1\rho}$ of the white matter: 76.07 ms, $T_{1\rho}$ of gray matter: 80.1 ms). And $T_{1\rho}$ measurements at 5.0 T showed no significant difference with that at 3.0 T, with the current imaging protocols. Theoretically, the chemical exchange and diffusion contribution to the $T_{1\rho}$ increases with the magnetic field, the field-dependent trend of the $T_{1\rho}$ relaxation times is less pronounced than that of T_1 in this study, which is similar to the T_2 relaxation times [43].

There were several limitations in this study. First, the scan time of $T_{1\rho}$ quantification is relatively long due to the requirement of acquiring multiple images with different TSLs. There might be a subject's motion during acquisition. Fast MRI techniques such as compressed sensing and deep learning can shorten the scan time to a clinically acceptable range but have not yet been integrated into the 5.0 T scanner. Second, the slice thickness is up to 3 mm in this study, which may cause some small lesions to be missed, or inaccurate characterization of lesions due to partial volume effects in clinical applications. Future technical improvement will focus on shortening the scan time for higher-resolution imaging by using the abovementioned fast MRI techniques. Third, all of the subjects were healthy volunteers, and no patient was included in this study. Since the $T_{1\rho}$ values of patients may be different from that of healthy volunteers, efforts should be made to further evaluate the $T_{1\rho}$ quantification of brain lesions at 5.0 T for patients with neurologic diseases and investigate the ability of $T_{1\rho}$ mapping to determine differences between normal and patients.

Conclusion

This study confirmed the feasibility of brain $T_{1\rho}$ quantification at 5.0 T. There was no significant difference between the brain $T_{1\rho}$ values obtained at 3.0 T and 5.0 T. The SNR of $T_{1\rho}$-weighted images was significantly improved at 5.0 T relative to 3.0 T, which is a benefit for high-resolution imaging and dispersion-related studies. The $T_{1\rho}$ quantification at 5.0 T may be reliable for clinical investigations.

Data availability statement

The original contributions presented in the study are included in the article/supplementary material, further inquiries can be directed to the corresponding authors.

Ethics statement

The studies involving human participants were reviewed and approved by the Ethics Committee at the Shenzhen Institute of Advanced Technology, Chinese Academy of Sciences (Ethics Committee approval number: YSB-2022-Y02088). The patients/participants provided their written informed consent to participate in this study.

Author contributions

YL: conceptualization, methodology, software, writing—original draft. WW: Formal analysis, data curation, visualization, writing—original draft. YZ: investigation, formal analysis, validation. HW: supervision. HZ: supervision. DL: supervision, writing—review and editing, funding acquisition. YZ: writing—review and editing, supervision, project administration, funding acquisition.

Funding

This study is supported by the National Key R&D Program of China no. 2020YFA0712200, National Natural Science Foundation of China under grant no. 62201561, 81971611, 62125111, 81901736, and U1805261, the Guangdong Basic and Applied Basic Research Foundation under grant no. 2021A1515110540, the Key Technology and Equipment R&D Program of Major Science and Technology Infrastructure of Shenzhen under grant no. 202100102, 202100104, Shenzhen Science and Technology Program under grant no. RCYX20210609104444089.

Conflict of interest

The authors declare that the research was conducted in the absence of any commercial or financial relationships that could be construed as a potential conflict of interest.

Publisher's note

All claims expressed in this article are solely those of the authors and do not necessarily represent those of their affiliated organizations, or those of the publisher, the editors and the reviewers. Any product that may be evaluated in this article, or claim that may be made by its manufacturer, is not guaranteed or endorsed by the publisher.

References

1. Wang YX, Zhang Q, Li X, Chen W, Ahuja A, Yuan J. T1ρ magnetic resonance: Basic physics principles and applications in knee and intervertebral disc imaging. *Quant Imaging Med Surg* (2015) 5:858–85. doi:10.3978/j.issn.2223-4292.2015.12.06

2. Jin T, Kim SG. Characterization of non-hemodynamic functional signal measured by spin-lock fMRI. *Neuroimage* (2013) 78:385–95. doi:10.1016/j.neuroimage.2013.04.045

3. Kettunen MI, Grohn OH, Silvennoinen MJ, Penttonen M, Kauppinen RA. Effects of intracellular pH, blood, and tissue oxygen tension on T1ρ relaxation in rat brain. *Magn Reson Med* (2002) 48:470–7. doi:10.1002/mrm.10233

4. Kettunen MI, Sierra A, Narvainen MJ, Valonen PK, Yla-Herttuala S, Kauppinen RA, et al. Low spin-lock field T1 relaxation in the rotating frame as a sensitive MR imaging marker for gene therapy treatment response in rat Glioma[1]. *Radiology* (2007) 243:796–803. doi:10.1148/radiol.2433052077

5. Magnotta VA, Heo HY, Dlouhy BJ, Dahdaleh NS, Follmer RL, Thedens DR, et al. Detecting activity-evoked pH changes in human brain. *Proc Natl Acad Sci U S A* (2012) 109:8270–3. doi:10.1073/pnas.1205902109

6. Gonyea JV, Watts R, Applebee A, Andrews T, Hipko S, Nickerson JP, et al. *In vivo* quantitative whole-brain T1ρ MRI of multiple sclerosis. *J Magn Reson Imaging* (2015) 42:1623–30. doi:10.1002/jmri.24954

7. Ma S, Wang N, Fan Z, Kaisey M, Sicotte NL, Christodoulou AG, et al. Three-dimensional whole-brain simultaneous T1, T2, and T1ρ quantification using MR Multitasking: Method and initial clinical experience in tissue characterization of multiple sclerosis. *Magn Reson Med* (2021) 85:1938–52. doi:10.1002/mrm.28553

8. Mangia S, Carpenter AF, Tyan AE, Eberly LE, Garwood M, Michaeli S. Magnetization transfer and adiabatic T1ρ MRI reveal abnormalities in normal-appearing white matter of subjects with multiple sclerosis. *Mult Scler* (2014) 20:1066–73. doi:10.1177/1352458513515084

9. Boles Ponto LL, Magnotta VA, Menda Y, Moser DJ, Oleson JJ, Harlynn EL, et al. Comparison of T_1Rho MRI, glucose metabolism, and amyloid burden across the cognitive spectrum: A pilot study. *J Neuropsychiatry Clin Neurosci* (2020) 32:352–61. doi:10.1176/appi.neuropsych.19100221

10. Borthakur A, Sochor M, Davatzikos C, Trojanowski JQ, Clark CM. T1ρ MRI of Alzheimer's disease. *Neuroimage* (2008) 41:1199–205. doi:10.1016/j.neuroimage.2008.03.030

11. Haris M, Yadav SK, Rizwan A, Singh A, Cai K, Kaura D, et al. T1rho MRI and CSF biomarkers in diagnosis of Alzheimer's disease. *NeuroImage: Clin* (2015) 7:598–604. doi:10.1016/j.nicl.2015.02.016

12. Haris M, Singh A, Cai KJ, Davatzikos C, Trojanowski JQ, Melhem ER, et al. T1rho (T1ρ) MR imaging in Alzheimer' disease and Parkinson's disease

with and without dementia. *J Neurol* (2011) 258:380–5. doi:10.1007/s00415-010-5762-6

13. Mangia S, Svatkova A, Mascali D, Nissi MJ, Burton PC, Bednarik P, et al. Multi-modal brain MRI in subjects with PD and iRBD. *Front Neurosci* (2017) 11:709. doi:10.3389/fnins.2017.00709

14. Nestrasil I, Michaeli S, Liimatainen T, Rydeen CE, Kotz CM, Nixon JP, et al. T1ρ and T2ρMRI in the evaluation of Parkinson's disease. *J Neurol* (2010) 257:964–8. doi:10.1007/s00415-009-5446-2

15. Jokivarsi KT, Hiltunen Y, Grohn H, Tuunanen P, Grohn OHJ, Kauppinen RA. Estimation of the onset time of cerebral ischemia using T1ρand T2 MRI in rats. *Stroke* (2010) 41:2335–40. doi:10.1161/strokeaha.110.587394

16. Tan YF, Xu J, Chen RY, Chen B, Xu J, Ren DK, et al. Use of T1 relaxation time in rotating frame (T1ρ) and apparent diffusion coefficient to estimate cerebral stroke evolution. *J Magn Reson Imaging* (2018) 48:1247–54. doi:10.1002/jmri.25971

17. Herz K, Gandhi C, Schuppert M, Deshmane A, Scheffler K, Zaiss M. CEST imaging at 9.4 T using adjusted adiabatic spin-lock pulses for on- and off-resonant T1ρ-dominated Z-spectrum acquisition. *Magn Reson Med* (2019) 81:275–90. doi:10.1002/mrm.27380

18. Paech D, Schuenke P, Koehler C, Windschuh J, Mundiyanapurath S, Bickelhaupt S, et al. T1ρ-weighted dynamic glucose-enhanced MR imaging in the human brain. *Radiology* (2017) 285:914–22. doi:10.1148/radiol.2017162351

19. Schuenke P, Koehler C, Korzowski A, Windschuh J, Bachert P, Ladd ME, et al. Adiabatically prepared spin-lock approach for T1ρ-based dynamic glucose enhanced MRI at ultrahigh fields. *Magn Reson Med* (2017) 78:215–25. doi:10.1002/mrm.26370

20. Spear JT, Gore JC. New insights into rotating frame relaxation at high field. *NMR Biomed* (2016) 29:1258–73. doi:10.1002/nbm.3490

21. Gilani IA, Sepponen R. Quantitative rotating frame relaxometry methods in MRI. *NMR Biomed* (2016) 29:841–61. doi:10.1002/nbm.3518

22. Jin T, Iordanova B, Hitchens TK, Modo M, Wang P, Mehrens H, et al. Chemical exchange-sensitive spin-lock (CESL) MRI of glucose and analogs in brain tumors. *Magn Reson Med* (2018) 80:488–95. doi:10.1002/mrm.27183

23. Chen WT, Chan Q, Wang YXJ. Breath-hold black blood quantitative T1rho imaging of liver using single shot fast spin echo acquisition. *Quant Imaging Med Surg* (2016) 6:168–77. doi:10.21037/qims.2016.04.05

24. Chen W. Artifacts correction for T1rho imaging with constant amplitude spin-lock. *J Magn Reson* (2017) 274:13–23. doi:10.1016/j.jmr.2016.11.002

25. Garwood M, DelaBarre L. The return of the frequency sweep: Designing adiabatic pulses for contemporary NMR. *J Magn Reson* (2001) 153:155–77. doi:10.1006/jmre.2001.2340

26. Johnson CP, Thedens DR, Kruger SJ, Magnotta VA. Three-Dimensional GRE T1ρ mapping of the brain using tailored variable flip-angle scheduling. *Magn Reson Med* (2020) 84:1235–49. doi:10.1002/mrm.28198

27. Li X, Han ET, Busse RF, Majumdar S. *In vivo* T1ρ mapping in cartilage using 3D magnetization-prepared angle-modulated partitioned k-space spoiled gradient echo snapshots (3D MAPSS). *Magn Reson Med* (2008) 59:298–307. doi:10.1002/mrm.21414

28. Wei Z, Chen Q, He Q, Zhang X, Liu X, zheng H, Li Y. A quadrature birdcage/48-channel receiver coil assembly for human brain imaging at 5T. In: 2022 Joint Annual Meeting ISMRM-ESMRMB & ISMRT 31st Annual Meeting; London (2022).

29. Zhu Y, Liu Y, Ying L, Peng X, Wang YJ, Yuan J, et al. SCOPE: Signal compensation for low-rank plus sparse matrix decomposition for fast parameter mapping. *Phys Med Biol* (2018) 63:185009. doi:10.1088/1361-6560/aadb09

30. Zhu Y, Liu Y, Ying L, Qiu Z, Liu Q, Jia S, et al. A 4-minute solution for submillimeter whole-brain T1ρ quantification. *Magn Reson Med* (2021) 85:3299–307. doi:10.1002/mrm.28656

31. Moré JJ. The levenberg-marquardt algorithm: Implementation and theory. *Numer Anal* (1978) 105–16. doi:10.1007/BFb0067700

32. Firbank MJ, Coulthard A, Harrison RM, Williams ED. A comparison of two methods for measuring the signal to noise ratio on MR images. *Phys Med Biol* (1999) 44:N261–4. doi:10.1088/0031-9155/44/12/403

33. Wyatt C, Guha A, Venkatachari A, Li XJ, Krug R, Kelley DE, et al. Improved differentiation between knees with cartilage lesions and controls using 7T relaxation time mapping. *J Orthopaedic Translation* (2015) 3:197–204. doi:10.1016/j.jot.2015.05.003

34. Springer E, Dymerska B, Cardoso PL, Robinson SD, Weisstanner C, Wiest R, et al. Comparison of routine brain imaging at 3 T and 7 T. *Invest Radiol* (2016) 51:469–82. doi:10.1097/rli.0000000000000256

35. Metcalf M, Xu D, Okuda DT, Carvajal L, Srinivasan R, Kelley DA, et al. High-resolution phased-array MRI of the human brain at 7 tesla: Initial experience in multiple sclerosis patients. *J Neuroimaging* (2010) 20:141–7. doi:10.1111/j.1552-6569.2008.00338.x

36. Zhang Y, Yang C, Liang L, Shi Z, Zhu S, Chen C, et al. Preliminary experience of 5.0 T higher field abdominal diffusion-weighted MRI: Agreement of apparent diffusion coefficient with 3.0 T imaging. *J Magn Reson Imaging* (2022). doi:10.1002/jmri.28097

37. Collins CM, Li S, Smith MB. SAR and B1 field distributions in a heterogeneous human head model within a birdcage coil. *Magn Reson Med* (1998) 40:847–56. doi:10.1002/mrm.1910400610

38. Li X, Han ET, Ma CB, Link TM, Newitt DC, Majumdar S. *In vivo* 3T spiral imaging based multi-slice T1ρ mapping of knee cartilage in osteoarthritis. *Magn Reson Med* (2005) 54:929–36. doi:10.1002/mrm.20609

39. Witschey WR, 2nd, Borthakur A, Elliott MA, Mellon E, Niyogi S, Wallman DJ, et al. Artifacts in $T_{1\rho}$-weighted imaging: Compensation for B1 and B0 field imperfections. *J Magn Reson* (2007) 186:75–85. doi:10.1016/j.jmr.2007.01.015

40. Charagundla SR, Borthakur A, Leigh JS, Reddy R. Artifacts in $T_{1\rho}$-weighted imaging: Correction with a self-compensating spin-locking pulse. *J Magn Reson* (2003) 162:113–21. doi:10.1016/s1090-7807(02)00197-0

41. Gram M, Seethaler M, Gensler D, Oberberger J, Jakob PM, Nordbeck P. Balanced spin-lock preparation for B1 -insensitive and B0 -insensitive quantification of the rotating frame relaxation time T1ρ. *Magn Reson Med* (2021) 85:2771–80. doi:10.1002/mrm.28585

42. Singh A, Haris M, Cai K, Kogan F, Hariharan H, Reddy R. High resolution T1ρ mapping of *in vivo* human knee cartilage at 7T. *Plos One* (2014) 9:e97486. doi:10.1371/journal.pone.0097486

43. Oros-Peusquens AM, Laurila M, Shah NJ. Magnetic field dependence of the distribution of NMR relaxation times in the living human brain. *Magn Reson Mater Phy* (2008) 21:131–47. doi:10.1007/s10334-008-0107-5

44. Grohn HI, Michaeli S, Garwood M, Kauppinen RA, Grohn OH. Quantitative T1ρ and adiabatic Carr-Purcell T2 magnetic resonance imaging of human occipital lobe at 4 T. *Magn Reson Med* (2005) 54:14–9. doi:10.1002/mrm.20536

45. Wheaton AJ, Borthakur A, Corbo M, Charagundla SR, Reddy R. Method for reduced SAR T1ρ-weighted MRI. *Magn Reson Med* (2004) 51:1096–102. doi:10.1002/mrm.20141